# FAST PARAMETER ESTIMATION ALGORITHM FOR CUBIC PHASE SIGNAL BASED ON QUANTIFYING EFFECTS OF DOPPLER FREQUENCY SHIFT

## Jibin Zheng[1, *], Tao Su[1], Qing Huo Liu[2], Long Zhang[1], and Wentao Zhu[1]

[1]National Lab of Radar Signal Processing, Xidian University, Xi'an 710071, China

[2]Department of Electrical and Computer Engineering, Duke University, Durham, NC 27708, USA

**Abstract**—For the chirp rate and its change rate estimation of cubic phase signal (CPS), conventional algorithms cannot achieve a trade-off between low computational cost and high performance. In this paper, by utilizing the numerical computational method (NCM), effects of Doppler frequency shift are quantified, and the relationships of the optimal signal length with the chirp rate and change rate of chirp rate are obtained. Then a fast parameter estimation algorithm (DMNUFFT), based on dechirp method (DM) and nonuniform fast Fourier transform (NUFFT), is proposed. Compared with existing algorithms, DMNUFFT can achieve high performance with relatively low computational cost. The performance analyses and an application to inverse synthetic aperture radar (ISAR) imaging are shown to validate the effectiveness of DMNUFFT.

## 1. INTRODUCTION

The chirp rate and its change rate are two important physical quantities of the cubic phase signal (CPS), and their estimations have a wide range of applications in radar, sonar, communication and acoustic [1–10]. The discrete-time noisy CPS can take the form below

$$s_z(n) = s(n) + z(n) = A_0 e^{\left[j2\pi\left(a_1(nT) + \frac{a_2}{2}(nT)^2 + \frac{a_3}{6}(nT)^3\right)\right]} + z(n) \quad (1)$$

for $-(N-1)/2 \leq n \leq (N-1)/2$, where $s(n)$ is the noise-free signal, $A_0$ is the constant amplitude, $N$ an odd integer representing the number

of samples, $T$ the sampling interval, $z(n)$ the additive complex white Gaussian noise with a variance of $\delta^2$, and $a_1$, $a_2$ and $a_3$ denote the centroid frequency, chirp rate and its change rate, respectively. The input signal-to-noise ratio (SNR) can be obtained as

$$\text{SNR}_{\text{input}} = 10 \log_{10} \frac{A_0^2}{\delta^2} \qquad (2)$$

In order to estimate these two parameters, many algorithms have been proposed, and they generally fall into two categories: correlation algorithms and non-correlation algorithms. The correlation algorithms include the higher-order ambiguity function (HAF) [1], cubic phase (CP) function [2, 3], higher-order ambiguity function-integrated cubic phase function (HAF-ICPF) [4], product generalized cubic phase function (PGCPF) [5], and parameters estimation algorithm based on non-uniformly spaced signal sample method [6]. The maximum likelihood (ML) method [7], and modified discrete chirp Fourier transform (DCFT) algorithm for CPS [8] belong to non-correlation algorithms. Correlation algorithms have lower computational cost ($O(N \log_2 N)$ or $O(N^2 \log_2 N)$, where $N$ is the effective signal length), but suffer from poor performance in the low SNRs. Compared with correlation algorithms, non-correlation algorithms are just the opposite, with higher performance, but higher computational load ($O(N^3 \log_2 N)$). It is worthwhile noting that all these algorithms above cannot achieve a trade-off between computational cost and anti-noise performance.

In this paper, a non-correlation algorithm, DMNUFFT, which is based on quantifying effects of Doppler frequency shift with the numerical computational method (NCM) [11, 12], is proposed. It utilizes dechirp method (DM) [13] and nonuniform fast Fourier transform (NUFFT) [14], and can be classed as an extension of the optimal ML algorithm. Given the advantage of NUFFT in computational cost, we also apply it to CPF and HAF-ICPF. With analyses of performance and computational cost, DMNUFFT is proved to be a more efficient algorithm, which can acquire high anti-noise performance with low computational cost.

## 2. THE EFFECT OF DOPPLER FREQUENCY SHIFT DUE TO CHIRP RATE AND CHANGE RATE OF CHIRP RATE

In this section, the NCM is utilized to quantify effects of Doppler frequency shift due to chirp rate and its change rate, and the relationships of the optimal signal length with the chirp rate and change rate of chirp rate will be obtained. The result, after using

the Fourier transform (FT) to $s(n)$, can be represented as

$$S(f) = \sum_{n=-\frac{N-1}{2}}^{\frac{N-1}{2}} A_0 e^{\left[j2\pi\left(a_1(nT)+\frac{a_2}{2}(nT)^2+\frac{a_3}{6}(nT)^3\right)\right]} e^{-j2\pi fnT} \quad (3)$$

If effects of the chirp rate and change rate of chirp rate are compensated, the maximum of $|S(f)|$ is

$$|S(f)|_{\max} = NA_0 \quad (4)$$

So the corresponding output SNR is

$$\mathrm{SNR}_{\mathrm{out,max}} = 10 \log_{10} \frac{NA_0^2}{\delta^2} \quad (5)$$

The $\mathrm{SNR}_{\mathrm{out,max}}$ with respect to $\mathrm{SNR}_{\mathrm{pulse}}$ gives the SNR gain

$$G_{\mathrm{SNR,max}} = \mathrm{SNR}_{\mathrm{out,max}} - \mathrm{SNR}_{\mathrm{pulse}} = 10 \log_{10} N \quad (6)$$

From (3), we know that the actual result of energy accumulation is affected by frequency Doppler shift due to the chirp rate and change rate of chirp rate. In the following, we will quantify effects of these two parameters.

## 2.1. Effect of the Chirp Rate Only

Assume the change rate of chirp rate is compensated. The noise-free signals $s(n)$ can be rewritten as

$$s_1(n) = A_0 e^{\left[j2\pi\left(a_1(nT)+\frac{a_2}{2}(nT)^2\right)\right]} \quad (7)$$

In (3), substitute $s(n)$ with $s_1(n)$

$$S_1(f) = \sum_{n=-\frac{N-1}{2}}^{\frac{N-1}{2}} A_0 e^{\left[j2\pi\left((a_1-f)(nT)+\frac{a_2}{2}(nT)^2\right)\right]} \quad (8)$$

The frequency of $s_1(n)$ can be described as

$$f = \frac{d\left[a_1(nT)+\frac{a_2}{2}(nT)^2\right]}{d(nT)} = a_1 + a_2(nT),$$

$$f \in \left[a_1 - a_2\left(\frac{N-1}{2}T\right), a_1 + a_2\left(\frac{N-1}{2}T\right)\right] \quad (9)$$

The frequency of $s_1(n)$ is around the midpoint $f_{\mathrm{mid}} = a_1$ and obeys the uniform distribution. So the energy distribution of $S_1(f)$ is symmetric. According to [11, 12], we know that there is a threshold

value $N_1$ for $N$. When $N < N_1$, the unique maximum of $|S_1(f)|$ is attained at $f = a_1$. Thus

$$
\max |S_1(f)| = |S_1(a_1)| = \left| \sum_{n=-\frac{N-1}{2}}^{\frac{N-1}{2}} A_0 e^{\left[ j2\pi \left( \frac{a_2}{2}(nT)^2 \right) \right]} \right| \tag{10}
$$

Figure 1(a) shows the $\max |S_1(f)|$ with different signal lengths when $a_2 = 60\,\text{Hz/s}$ and $T = 1/600\,\text{s}$. In Figure 1(b), we select several representative signal lengths from Figure 1(a) to plot the $|S_1(f)|$.

In Figure 1, when $a_2 = 60\,\text{Hz/s}$ and $T = 1/600\,\text{s}$, the threshold value $N_1$ is 169 and the optimal value $N_{1,\text{opt}}$ is 133. For a given chirp rate $a_2$, the maximum output SNR can be obtained when the signal length is equal to its corresponding optimal value $N_{1,\text{opt}}$, which benefits the target detection and parameter estimation. Thus, with (6) and (10), the output SNR, optimal SNR gain and loss of SNR gain with respect to optimal signal length can be represented as

$$
\text{SNR}_{\text{out},1,\text{opt}} = 10 \log_{10} \frac{A_0^2}{N_{1,\text{opt}}\delta^2} \left| \sum_{n=-\frac{N_{1,\text{opt}}-1}{2}}^{\frac{N_{1,\text{opt}}-1}{2}} A_0 e^{\left[ j2\pi \left( \frac{a_2}{2}(nT)^2 \right) \right]} \right|^2 \tag{11}
$$



(a)                                                     (b)
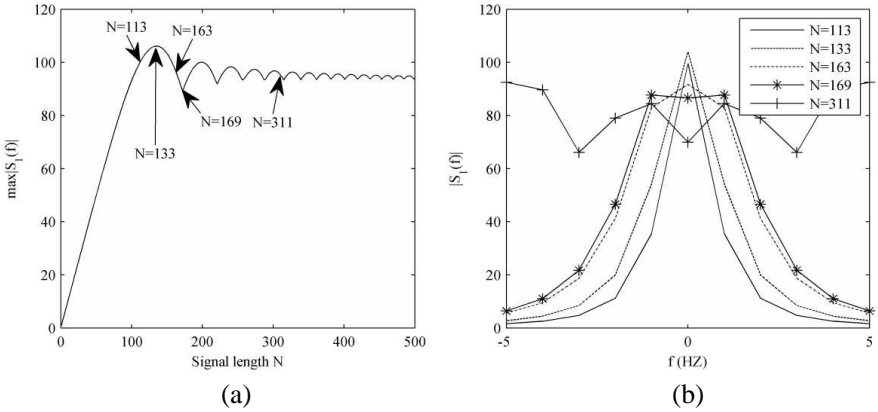
**Figure 1.** Simulation results when $a_2 = 60\,\text{Hz/s}$, $T = 1/600\,\text{s}$. (a) $\max |S_1(f)|$ with different signal lengths. (b) $|S_1(f)|$ with the signal lengths marked in (a).

$$G_{\mathrm{SNR},1,\mathrm{opt}} = 10\log_{10}\frac{1}{N_{1,\mathrm{opt}}}\left|\sum_{n=-\frac{N_{1,\mathrm{opt}}-1}{2}}^{\frac{N_{1,\mathrm{opt}}-1}{2}}A_0 e^{\left[j2\pi\left(\frac{a_2}{2}(nT)^2\right)\right]}\right|^2 \qquad (12)$$

$$\Delta G_{\mathrm{SNR},1,\mathrm{opt}} = G_{\mathrm{SNR},\max} - G_{\mathrm{SNR},1,\mathrm{opt}}$$

$$= 10\log_{10}N_{1,\mathrm{opt}} - 10\log_{10}\frac{1}{N_{1,\mathrm{opt}}}\left|\sum_{n=-\frac{N_{1,\mathrm{opt}}-1}{2}}^{\frac{N_{1,\mathrm{opt}}-1}{2}}A_0 e^{\left[j2\pi\left(\frac{a_2}{2}(nT)^2\right)\right]}\right|^2 \quad (13)$$

However, it is difficult to obtain the analytical relationship of the optimal value with the chirp rate. Therefore, NCM is utilized to obtain the approximation relationships. For a given $a_2$, we calculate $N_{1,\mathrm{opt}}$ and $G_{\mathrm{SNR},1,\mathrm{opt}}$ by (10) and (12). We plot points $(10\log_{10}N_{1,\mathrm{opt}},\ 10\log_{10}a_2)$ in Figure 2(a) and points $(G_{\mathrm{SNR},1,\mathrm{opt}},\ 10\log_{10}a_2)$ in Figure 2(b). With the linear least squares (LLS) fit [12], the relationships of $N_{1,\mathrm{opt}}$ and $G_{\mathrm{SNR},1,\mathrm{opt}}$ with $a_2$ can be obtained as

$$10\log_{10}N_{1,\mathrm{opt}} = -\frac{10\log_{10}a_2}{2} + 30.1 \qquad (14)$$

$$G_{\mathrm{SNR},1,\mathrm{opt}} = -\frac{10\log_{10}a_2}{2} + 28 \qquad (15)$$

In Figure 2(b), the results of matched filter are also plotted with the same signal lengths and the loss of SNR gain is

$$\Delta G_{\mathrm{SNR},1,\mathrm{opt}} = 2.1\,(\mathrm{dB}) \qquad (16)$$
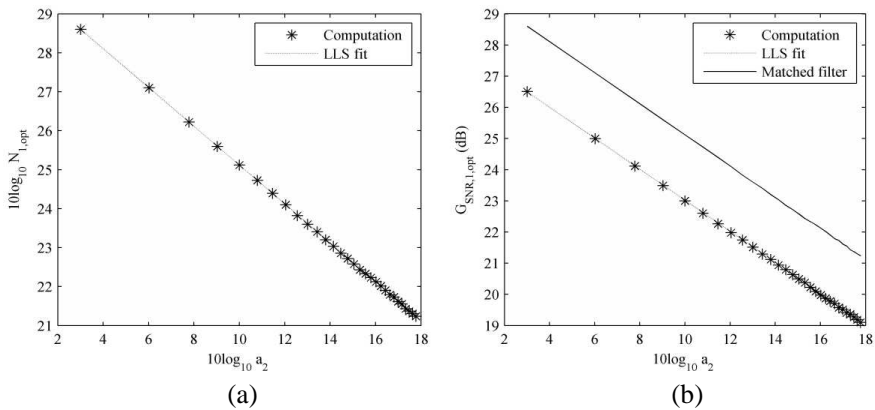


**Figure 2.** The relationships of the optimal value and SNR gain with the chirp rate when $T = 1/600\,\mathrm{s}$. (a) The relationships of the optimal signal length with the chirp rate. (b) The relationships of the optimal SNR gain with the chirp rate.

For the results above, if the sampling interval is altered but the optimal value is the same, we still can obtain the corresponding chirp rate based on the result of $T = 1/600\,\text{s}$. For example, if the sampling interval of another CPS is $T_{\text{ano}}$, its corresponding chirp rate $a_{2,\text{ano}}$ should be $a_2 T / T_{\text{ano}}$. Based on the analyses of Subsections 2.2 and 2.3 below, we also find that same relationships are also tenable.

## 2.2. Effect of the Change Rate of Chirp Rate Only

Assume the chirp rate is compensated. The noise-free signal $s(n)$ can be rewritten as

$$s_2(n) = A_0 e^{\left[j2\pi\left(a_1(nT) + \frac{a_3}{6}(nT)^3\right)\right]} \tag{17}$$

In (3), substitute $s(n)$ with $s_2(n)$

$$S_2(f) = \sum_{n=-\frac{N-1}{2}}^{\frac{N-1}{2}} A_0 e^{\left[j2\pi\left((a_1-f)(nT) + \frac{a_3}{6}(nT)^3\right)\right]} \tag{18}$$

The frequency of $s_2(n)$ can be described as

$$f = \frac{d\left[a_1(nT) + \frac{a_3}{6}(nT)^3\right]}{d(nT)} = a_1 + \frac{a_3}{2}(nT)^2,$$

$$f \in \left[a_1, a_1 + \frac{a_3}{2}\left(\frac{N-1}{2}T\right)^2\right] \tag{19}$$

The frequency of $s_2(n)$ does not obey the uniform distribution and the energy of $S_2(f)$ spreads only in one direction due to the mono-direction of the Doppler frequency shift. This is similar to the effect of acceleration in the radar signal processing. So according to the principle of radar signal processing [15, 16], we know that there is a threshold value $N_2$ for $N$. When $N < N_2$, the unique maximum of $|S_2(f)|$ is attained at $f = a_1$. Thus, when $N < N_2$, we obtain

$$\max |S_2(f)| = |S_2(a_1)| = \sum_{n=-\frac{N-1}{2}}^{\frac{N-1}{2}} A_0 e^{\left[j2\pi\left(\frac{a_3}{6}(nT)^3\right)\right]} \tag{20}$$

Figure 3(a) shows the $\max |S_2(f)|$ with different signal lengths when $a_3 = 120\,\text{Hz/s}$ and $T = 1/600\,\text{s}$. In Figure 3(b), we select several representative signal lengths from Figure 3(a) to plot the $|S_2(f)|$.

In Figure 3, the threshold value $N_2$ and optimal value $N_{2,\text{opt}}$ are 337 and 279, respectively. Due to the non-uniform distribution of
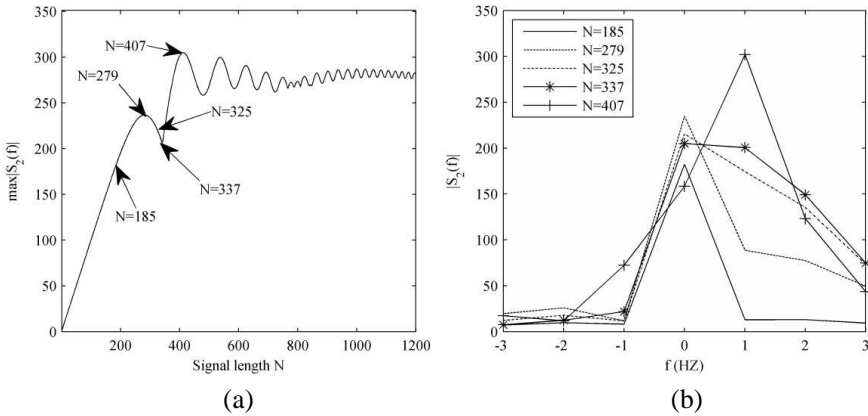
**Figure 3.** Simulation results when $a_3 = 120\,\text{Hz/s}$, $T = 1/600\,\text{s}$. (a) max $|S_2(f)|$ with different signal lengths. (b) $|S_2(f)|$ with the signal lengths marked in (a).

frequency and the mono-direction of the Doppler frequency shift, a better result appears when $N = 407$. However this result appears when $f \neq a_1$, which is not expected and not suitable for DM [13]. With (6) and (20), the output SNR, SNR gain and loss of SNR gain with respect to optimal signal length can be represented as

$$\text{SNR}_{\text{out},2,\text{opt}} = 10 \log_{10} \frac{A_0^2}{N_{2,\text{opt}}\delta^2} \left| \sum_{n=-\frac{N_{2,\text{opt}}-1}{2}}^{\frac{N_{2,\text{opt}}-1}{2}} e^{\left[j2\pi\left(\frac{a_3}{6}(nT)^3\right)\right]} \right|^2 \tag{21}$$

$$G_{\text{SNR},2,\text{opt}} = 10 \log_{10} \frac{1}{N_{2,\text{opt}}} \left| \sum_{n=-\frac{N_{2,\text{opt}}-1}{2}}^{\frac{N_{2,\text{opt}}-1}{2}} e^{\left[j2\pi\left(\frac{a_3}{6}(nT)^3\right)\right]} \right|^2 \tag{22}$$

$$\Delta G_{\text{SNR},2,\text{opt}} = G_{\text{SNR,max}} - G_{\text{SNR},2,\text{opt}}$$

$$= 10\log_{10} N_{2,\text{opt}} - 10\log_{10} \frac{1}{N_{2,\text{opt}}} \left| \sum_{n=-\frac{N_{2,\text{opt}}-1}{2}}^{\frac{N_{2,\text{opt}}-1}{2}} e^{\left[j2\pi\left(\frac{a_3}{6}(nT)^3\right)\right]} \right|^2 \tag{23}$$

NCM is also utilized to obtain approximation relationships of the optimum signal length with $a_3$. For a given $a_3$, we can calculate the corresponding $N_{2,\text{opt}}$ and $G_{\text{SNR},2,\text{opt}}$. We plot points $(10\log_{10} N_{2,\text{opt}}, 10\log_{10} a_3)$ in Figure 4(a) and points $(G_{\text{SNR},2,\text{opt}}, 10\log_{10} a_3)$ in Figure 4(b). With the LLS fit, the relationships of $N_{1,\text{opt}}$ and $G_{\text{SNR},1,\text{opt}}$
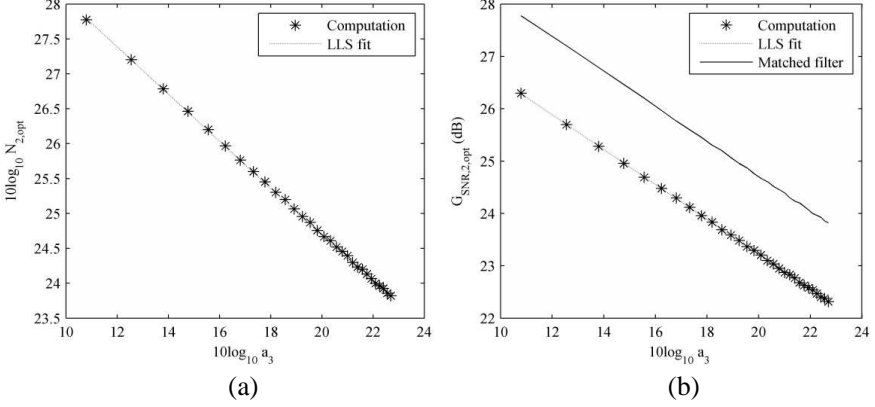
**Figure 4.** The relationships of the optimal value and SNR gain with the change rate of chirp rate when $T = 1/600\,\text{s}$. (a) The relationships of the optimal signal length with the change rate of chirp rate. (b) The relationships of the optimal SNR gain with the change rate of chirp rate.

with $a_2$ can be obtained as

$$10 \log_{10} N_{2,\text{opt}} = -\frac{10 \log_{10} a_3}{3} + 31.4 \tag{24}$$

$$G_{\text{SNR},2,\text{opt}} = -\frac{10 \log_{10} a_3}{3} + 30 \tag{25}$$

In Figure 4(b), the results of the matched filter are plotted. We can see that when the signal length $N$ equals $N_{2,\text{opt}}$, the loss of SNR gain is

$$\Delta G_{\text{SNR},2} = 1.4\,(\text{dB}) \tag{26}$$

## 2.3. Effects of Both the Chirp Rate and Change Rate of Chirp Rate

Assume both the parameters are not compensated. Rewrite (3) as

$$S_3(f) = \sum_{n=-\frac{N-1}{2}}^{\frac{N-1}{2}} A_0 e^{\left[j2\pi\left((a_1-f)(nT) + \frac{a_2}{2}(nT)^2 + \frac{a_3}{6}(nT)^3\right)\right]} \tag{27}$$

The frequency of $s(n)$ can be described as

$$f = \frac{d\left[a_1(nT) + \frac{a_2}{2}(nT)^2 + \frac{a_3}{6}(nT)^3\right]}{d(nT)} = a_1 + a_2(nT) + \frac{a_3}{2}(nT)^2 \tag{28}$$

The frequency in (28) inherits the characteristics of (9) and (19) and the optimal value $N_{\text{opt}}$ for $N$ also exist. When $N = N_{\text{opt}}$, the corresponding maximum of $|S_3(f)|$ is

$$\max |S_3(f)| = \sum_{n=-\frac{N_{\text{opt}}-1}{2}}^{\frac{N_{\text{opt}}-1}{2}} A_0 e^{\left[j2\pi\left(\frac{a_2}{2}(nT)^2+\frac{a_3}{6}(nT)^3\right)\right]} \qquad (29)$$

Then the NCM is utilized to obtain the relationships of the optimum signal length $N_{\text{opt}}$ with the given chirp rate and change rate of chirp rate. The relationships are shown in Figure 5.

Through the results of NCM in Figure 5, we find that four ridges appear. The optimal signal length will be increased when the parameters get close to the ridges, parallelly or vertically. The appearance of four ridges promotes us to consider how to set the search step lengths of chirp rate and its change rate, if the DM is used. For example, we set the step length $6\,\text{Hz/s}$ for $a_2$ and $40\,\text{Hz/s}^2$ for $a_3$, respectively, when the signal length is 687. After DM, the rest parameters after compensation are assumed to be $0\,\text{Hz/s}$ for $a_2$ and $40\,\text{Hz/s}^2$ for $a_3$, respectively. According to the analyses in the Subsection 2.1, the unique maximum of $|S_3(f)|$ will not be attained when $f = a_1$. Based on the results of Figure 5, we know that the minimum optimal value of a search range happens on the coordinate. Considering this, the search step length should be set according to



(a)

(b)
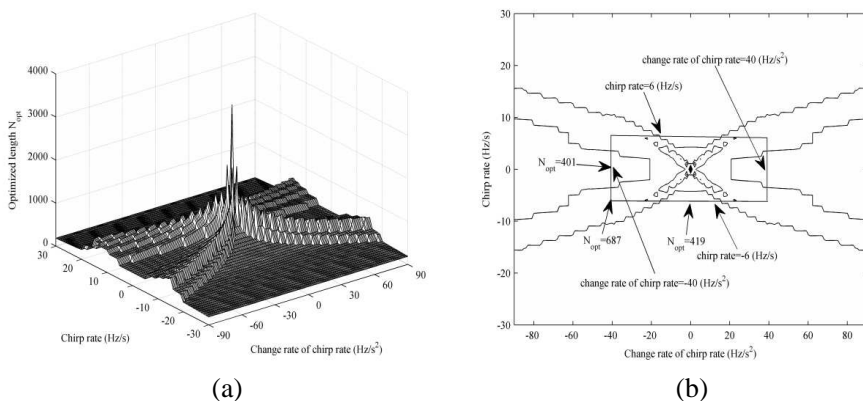
**Figure 5.** The relationships of the optimum signal length with the chirp rate and change rate of chirp rate when $T = 1/600\,\text{s}$. (a) Stereogram of the relationships. (b) Contour of the relationships.

the signal length $N$. So the corresponding search step length can be obtained based on (14) and (24).

$$a_{2,N} = 10^{(6.02-2\log_{10} N)}, \quad a_{3,N} = 10^{(9.42-3\log_{10} N)} \tag{30}$$

With (30), the output SNR, SNR gain and loss of SNR gain with respect to signal length $N$ can be represented as

$$\text{SNR}_{\text{out}} = 10\log_{10} \frac{A_0^2}{N\delta^2} \left| \sum_{n=-\frac{N-1}{2}}^{\frac{N-1}{2}} e^{\left[ j2\pi \left( \frac{a_{2,N}}{2}(nT)^2 + \frac{a_{3,N}}{6}(nT)^3 \right) \right]} \right|^2 \tag{31}$$
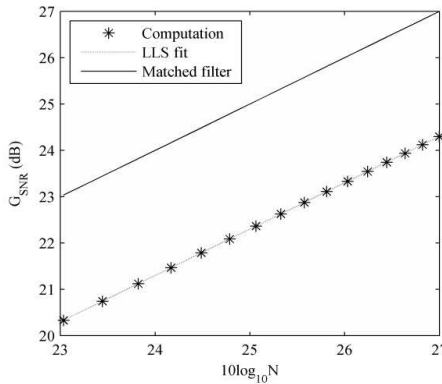
$$G_{\text{SNR}} = 10\log_{10} \frac{1}{N} \left| \sum_{n=-\frac{N-1}{2}}^{\frac{N-1}{2}} e^{\left[ j2\pi \left( \frac{a_{2,N}}{2}(nT)^2 + \frac{a_{3,N}}{6}(nT)^3 \right) \right]} \right|^2 \tag{32}$$

$$\Delta G_{\text{SNR}} = G_{\text{SNR,max}} - G_{\text{SNR}}$$

$$= 10\log_{10} N - 10\log_{10} \frac{1}{N} \left| \sum_{n=-\frac{N-1}{2}}^{\frac{N-1}{2}} e^{\left[ j2\pi \left( \frac{a_{2,N}}{2}(nT)^2 + \frac{a_{3,N}}{6}(nT)^3 \right) \right]} \right|^2 \tag{33}$$

Points $(G_{\text{SNR}}, 10\log_{10} N)$ are plotted in Figure 6 and also formed into a straight line. Using the LLS method, we get

$$G_{\text{SNR}} = 10\log_{10} N - 2.7 \tag{34}$$



**Figure 6.** The relationships of the signal length with SNR gain when $T = 1/600$ s.

In Figure 6, the results of the matched filter are also plotted. The corresponding SNR gain loss is

$$\Delta G_{\text{SNR}} = 2.7 \, (\text{dB}) \tag{35}$$

## 3. DMNUFFT ALGORITHM

In Section 2, the relationships of the optimal signal length with the chirp rate and its change rate are obtained. For any given signals, based on the obtained relationships, we can determine the search step lengths for chirp rate and change rate of chirp rate in the application of DM. So the DMNUFFT algorithm is proposed with the DM and NUFFT. The process of the DMNUFFT algorithm can be summarized as follows.

*Step 1.* According to the signal length $N$, sampling interval $T$ and (30), the search step lengths for the chirp rate and its change rate can be calculated as $a_{2,\text{step}}$ and $a_{3,\text{step}}$ respectively.

$$a_{2,\text{step}} = \frac{1}{300T} 10^{(6-2\log_{10} N)}, \quad a_{3,\text{step}} = \frac{1}{300T} 10^{(9.42-3\log_{10} N)} \tag{36}$$

*Step 2.* Initiate the chirp rate and its change rate as $a_{2,\text{init}}$ and $a_{3,\text{init}}$ respectively. Construct a dechirp function

$$D(\gamma, k) = e^{\left[-j2\pi\left(\frac{a_{2,\text{init}}+\gamma a_{2,\text{step}}}{2}(nT)^2 + \frac{a_{3,\text{init}}+k a_{3,\text{step}}}{6}(nT)^3\right)\right]} \tag{37}$$

for $-K \leq k \leq K$, $-R \leq \gamma \leq R$, $2K$ and $2R$ are the number of chirp rate and its change rate search needed respectively.

*Step 3.* Multiply (37) with $s_z(n)$

$$s_{z,\text{com}}(n, \gamma, k)$$
$$= A_0 e^{\left[j2\pi\left(a_1(nT) + \left(\frac{a_2}{2} - \frac{a_{2,\text{init}}+\gamma a_{2,\text{step}}}{2}\right)(nT)^2 + \left(\frac{a_3}{6} - \frac{a_{3,\text{init}}+k a_{3,\text{step}}}{6}\right)(nT)^3\right)\right]} + z_1(n) \tag{38}$$

where $z_1(n)$ is the noise after multiplied with (37).

*Step 4.* Create a cost function to estimate the parameters

$$(a_{1,\text{fine}}, \gamma_{\text{opt}}, k_{\text{opt}}) = \arg\max_{\gamma_i}\left\{\arg\max_{k_h} |\text{FFT}[s_{z,\text{com}}(n, \gamma_i, k_h)]|\right\} \tag{39}$$

where $a_{1,\text{fine}}$ is the accurate estimation of centroid frequency. Thus, we acquire the coarse estimation of $a_{2,\text{coar}}$ and $a_{3,\text{coar}}$

$$a_{2,\text{coar}} = a_{2,\text{init}} + \gamma_{\text{opt}} a_{2,\text{step}}, \quad a_{3,\text{coar}} = a_{3,\text{init}} + k_{\text{opt}} a_{3,\text{step}} \tag{40}$$

*Step 5.* Based on the estimated $a_{1,\text{fine}}$, $a_{2,\text{coar}}$ and fine step length $a_{2,\text{step,fine}}$ to construct another dechirp function

$$D_{\text{coar}}(g) = e^{\left[-j2\pi\left(a_{1,\text{fine}}(nT) + \frac{a_{2,\text{coar}}+g a_{2,\text{step,fine}}}{2}(nT)^2\right)\right]} \tag{41}$$

multiply (41) with $s_z(n)$

$$s_{z,\text{com},1}(n,g)$$

$$\approx A_0 e^{\left[j2\pi\left(\left(\frac{a_2}{2} - \frac{a_{2,\text{coar}} + ga_{2,\text{step,fine}}}{2}\right)(nT)^2 + \frac{a_3}{6}(nT)^3\right)\right]} + z_3(n) \qquad (42)$$

for $-G \leq g \leq G$, where $2G$ is the number of chirp rate search needed, $z_3(n)$ is the noise after multiplied with (41).

*Step 6.* Considering the computational cost [14] and result of energy accumulation [17], we perform NUFFT corresponding to $a_3$. Then combined with (42), the cost function can be constructed as follows

$$(g_{\text{opt}}, a_{3,\text{fine}}) = \arg\max_{g_j} \left|\text{NUFFT}_{(nT)^3}[s_{z,\text{com},1}(n, g_j)]\right| \qquad (43)$$

where $\text{NUFFT}_{(nT)^3}(\cdot)$ denotes NUFFT operator with respect to $(nT)^3$.

So the accurate estimation of the chirp rate can be represented as

$$a_{2,\text{fine}} = a_{2,\text{coar}} + g_{\text{opt}} a_{2,\text{step,fine}} \qquad (44)$$

Above is the DMNUFFT algorithm based on the analyses in Section 2. The computational cost is reduced a lot compared with ML method and MDCFT due to the obtained search step length and NUFFT. We use the number of complex multiplication to analyze the computational complexity. According to the analyses above, the computational cost of the DMNUFFT is about $O[(4KR + 2G)N\log_2 N]$. For example, when the signal length $N$ is 401 and sampling frequency $f_s$ is 600 Hz, the number of complex multiplication is about $O(N^2 \log N)$. In Section 2, compared with matched filter, the biggest SNR gain loss of DMNUFFT is about 2.7 dB. Thus, DMNUFFT is more suitable for the real world application due to low computational cost and high performance.

# 4. ANALYSES OF MEAN SQUARE ERROR AND INPUT-OUTPUT SNR

We consider one CPS denoted by $Au$. The sampling frequency $F_s$ is 600 Hz, and the effective signal length $N$ is equal to 401. Signal parameters are set as follows: $A_0 = 1$, $a_1 = 240$, $a_2 = 150$, $a_3 = 78$ for $Au$.

Based on (36) and sampling frequency, the search range of DM can be set as $[-405, -390, \ldots, -15, 0, 15, \ldots, 390, 405]$ Hz/s for $a_2$, $[-1200, -1120, \ldots, -80, 0, 80, \ldots, 1120, 1200]$ Hz/s$^2$ for $a_3$. For the nonuniformly spaced signal, NUFFT is better in computation cost, resolution and performance than dechirp method and discrete Fourier transform (DFT), so we apply NUFFT to CPF and HAF-ICPF. Then

CPF based on NUFFT and HAF-ICPF based on NUFFT are chosen to compare performance with NUFFT. We utilize mean square error (MSE) and input-output SNR to evaluate the DMNUFFT algorithm. The input SNRs tested in Figure 7 are $\text{SNR}_{\text{in}} = [-15 : 1 : 0]$ and for each input SNR, 500 trials are performed.

DMNUFFT belongs to non-correlation algorithm, while CPF based on NUFFT and HAF-ICPF based on NUFFT belong to correlation algorithm. Thus, in Figure 7, the threshold SNR is $-11\,\text{dB}$ for DMNUFFT, and $-3\,\text{dB}$ for CPF based on NUFFT and HAF-ICPF based on NUFFT. Even in high SNRs, DMNUFFT obtains better results than the other two algorithms due to the reduced noise influence
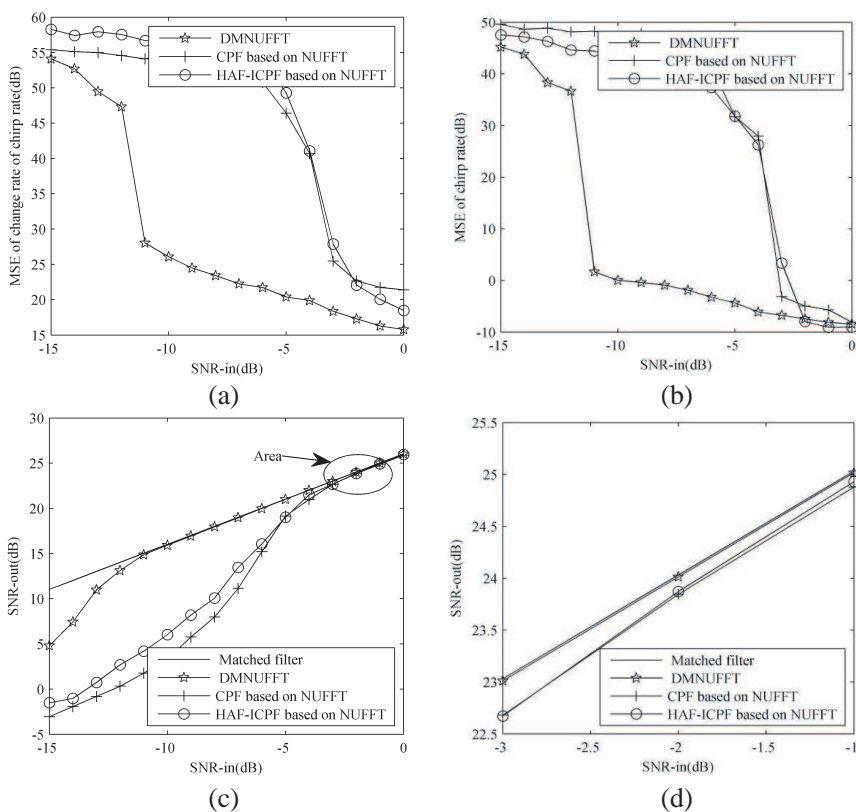


**Figure 7.** Performance comparison with $Au_1$. (a) MSE of the chirp rate estimation. (b) MSE of the change rate of chirp rate estimation. (c) Performance of input-output SNR. (d) Zoomed-in plot of the area in (c).

and no error propagation. The result of HAF-ICPF based on NUFFT is no better than that of the CPF based on NUFFT, but the HAF-ICPF based on NUFFT is more suitable for multi-components CPS.

## 5. ISAR IMAGING WITH DMNUFFT

ISAR imaging is one of the important high-resolution radar applications for moving targets. The radial acceleration, acceleration rate, angular acceleration, and angular acceleration rate of targets will lead the echo signal to be a CPS along the azimuth bin, which degrades the imaging quality. After the migration compensation, initial distance compensation and range compression [18–22], the complex range profile can be represented as

$$
S\left(t, t_{m}\right)
$$
$$
= B \sin c \left[ B \left( t - \frac{2 x_{p}}{c} \right) \right] e^{j 2 \pi \left( a_{1} t_{m} + \frac{a_{2}}{2} t_{m}^{2} + \frac{a_{3}}{6} t_{m}^{3} \right)} \mathrm{rect}\left( \frac{t_{m}}{T_{\mathrm{ob}}} \right) + z\left(t, t_{m}\right) \quad (45)
$$

where $a_{1} = (2 f_{c}/c)(v_{r} + y_{p} w_{1})$, $a_{2} = (2 f_{c}/c)(a_{r} + y_{p} w_{2})$, $a_{3} = (2 f_{c}/c)(\gamma_{r} + y_{p} w_{3})$, $t$ is the fast time, $t_{m}$ is the slow time, $(x_{p}, y_{p})$ is the initial coordinate, $f_{c}$ represents the carrier frequency, $B$ is the transmitted signal bandwidth, $c$ is the speed of light, $T_{\mathrm{ob}}$ is the observation time, $v_{r}$, $a_{r}$, and $\gamma_{r}$ are the radial velocity (without velocity ambiguity), acceleration, and acceleration rate, $w_{1}$, $w_{2}$, and $w_{3}$ are the initial angular velocity, angular acceleration, and angular acceleration rate, $z(t, t_{m})$ is additive complex white Gaussian noise with a variance of $\delta^{2}$.

In order to improve the image quality, we should estimate $a_{2}$ and $a_{3}$, and utilize them to compensate the Doppler frequency shift. Below we utilize the DMNUFFT to obtain the ISAR image. The target is a simulated aircraft shown in Figure 8(a). The parameters
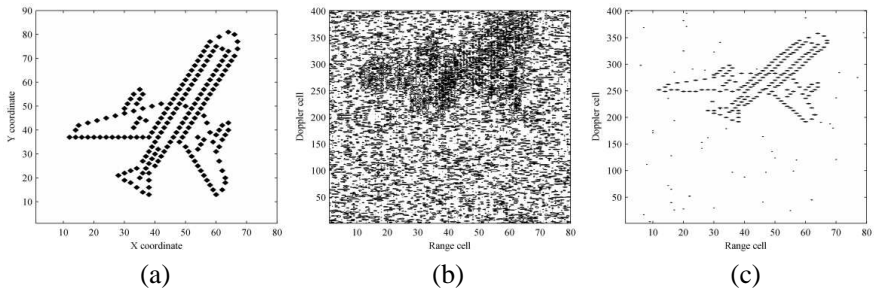


**Figure 8.** ISAR Imag for maneuvering target. (a) Target model. (b) ISAR image based on the RD algorithm. (c) ISAR image based on the DMNUFFT algorithm.

of radar and moving targets are listed in Table 1. Figure 8(b) is the results of conventional range-Doppler (RD) method and the results of DMNUFFT is shown in Figure 8(c).

**Table 1.** Radar parameters and moving parameters of target.

| Carrier frequency $f_c$ | 5 GHz | Radial velocity $v$ | 162 m/s |
|---|---|---|---|
| Bandwidth $B$ | 150 MHz | Acceleration $a_r$ | 6 m/s$^2$ |
| Sample frequency $f_s$ | 150 MHz | Acceleration rate $\gamma_r$ | 3 m/s$^3$ |
| Pulse number | 401 | Angular velocity $w_1$ | 0.09 rad/s |
| SNR after pulse compression | −6 dB | Angular acceleration $w_2$ | 0.03 rad/s$^2$ |
| Pulse Repetition frequency | 1000 Hz | Angular acceleration rate $w_3$ | 0.015 rad/s$^3$ |

In Figure 8(b), the energy is spread in azimuth cell due to the chirp rate and its change rate, so the imaging quality is degraded. With the DMNUFFT, the chirp rate and its change rate can be estimated, and then Doppler frequency shift can be compensated. Figure 8(c) shows the validity of the DMNUFFT.

Below we use the real radar data of a ship to demonstrate the effectiveness of DMNUFFT. For the real radar data, the carrier frequency is 15.4 GHz, Bandwidth is 80 MHz, Pulse number is 211, and Pulse Repetition frequency is 500 Hz. Figure 9(a) is the processing result of RD algorithm and the processing results of DMNUFFT are
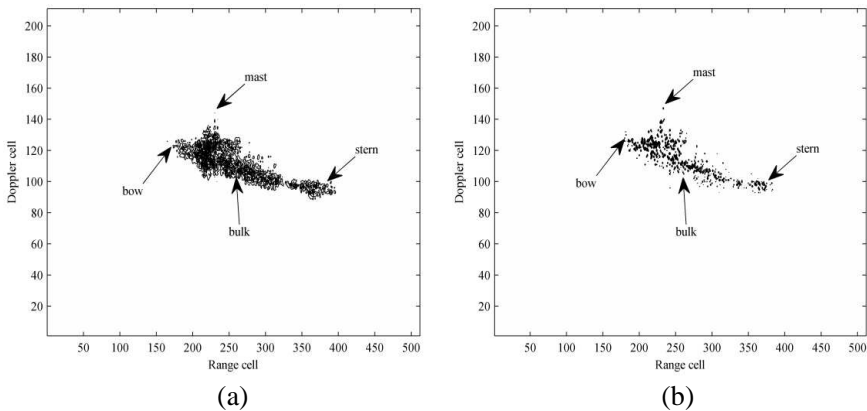


**Figure 9.** Processing results of the real radar data. (a) ISAR image based on the RD algorithm. (b) ISAR image based on DMNUFFT.

shown in Figure 9(b).

Compared with the results of RD algorithm in Figure 9(a), the quality of ISAR image in Figure 9(b) is improved a lot, and it's easy to discern the mast, bow, stern, etc. in ship. This is because, with the proposed algorithm, Doppler frequency shift due to the chirp rate and its change rate is compensated in the lower SNR.

## 6. CONCLUSION

Based on the results of quantifying effects of Doppler frequency shift, DMNUFFT is proposed. This algorithm can be classed as an extension of the optimal ML algorithm due to three-dimensional (3D) maximization, while performance analyses and ISAR imaging results prove that DMNUFFT achieves a trade-off between computational cost and anti-noise performance, and is more suitable for real world.

## ACKNOWLEDGMENT

## REFERENCES

1. Peleg, S. and P. Porat, "Linear FM signal parameter estimation from discrete-time observations," *IEEE Trans. Aerosp. Electron. Syst.*, Vol. 27, No. 4, 607–616, Jul. 1991.

2. O'Shea, P., "A new technique for instantaneous frequency rate estimation," *IEEE Signal Process. Lett.*, Vol. 9, No. 8, 251–252, Aug. 2002.

3. O'Shea, P., "A fast algorithm for estimating the parameters of a quadratic FM signal," *IEEE Trans. Signal Process.*, Vol. 52, No. 2, 385–393, Feb. 2004.

4. Wang, Y. and Y. C. Jiang, "ISAR imaging of a ship target using product high order matched-phase transform," *IEEE Geosci. Remote Sens. Lett.*, Vol. 6, No. 4, 658–661, Jun. 2009.

5. Wang, Y., "Inverse synthetic aperture radar imaging of manoeuvring target based on range-instantaneous-Doppler and range-instantaneous-chirp-rate algorithms," *IET Radar, Sonar and Navigation*, Vol. 6, No. 9, 921–928, Jul. 2012.

6.  Wang, Y. and Y. Jiang, "Inverse synthetic aperture radar imaging of manoeuvring target based on the product generalized cubic phase function," *IEEE Geosci. Remote Sens. Lett.*, Vol. 8, No. 5, 958–962, Sep. 2011.

7.  O'Shea, P., "Improving polynomial phase parameter estimation by using nonuniformly spaced signal sample method," *IEEE Trans. Signal Process.*, Vol. 60, No. 7, 3405–3414, Jul. 2012.

8.  Li, Y., R. Wu, M. Xing, and Z. Bao, "Inverse synthetic aperture radar imaging of ship target with complex motion," *IET Radar, Sonar and Navigation*, Vol. 2, No. 6, 395–403, Feb. 2008.

9.  Yuan, X., "Direction-finding wideband linear FM sources with triangular arrays," *IEEE Trans. Aerosp. Electron. Syst.*, Vol. 48, No. 3, 2416–2425, Jul. 2012.

10. Yuan, X., "Estimating the DOA and the polarization of a polynomial-phase signal using a single polarized vector-sensor," *IEEE Trans. Signal Process.*, Vol. 60, No. 3, 1270–1282, Mar. 2012.

11. Abatzoglou, T. J., "Fast maximum likelihood joint estimation of frequency and frequency rate," *IEEE Trans. Aerosp. Electron. Syst.*, Vol. 22, No. 6, 708–715, Nov. 1986.

12. Wu, L., X. Wei, D. Yang, H. Wang, and X. Li, "ISAR imaging of targets with complex motion based on discrete chirp Fourier transform for cubic chirps," *IEEE Trans. Geosci. Remote Sens.*, Vol. 50, No. 10, 4201–4212, Oct. 2012.

13. Tao, R., N. Zhang, and Y. Wang, "Analysing and compensating effects of range and Doppler frequency migrations in linear frequency modulation pulse compression radar," *IET Radar, Sonar and Navigation*, Vol. 5, No. 1, 12–22, Jan. 2011.

14. Yasotharan, A. and T. Thayaparan, "Strengths and limitations of the Fourier method for detecting acceleration targets by pulse Doppler radar," *IEE Proc. Radar, Sonar and Navigation*, Vol. 149, No. 2, 83–88, Apr. 2002.

15. Peng, X., W. Tan, Y. Wang, W. Hong, and Y. Wu, "Convolution back-projection imaging algorithm for downward-looking sparse linear array three dimensional synthetic aperture radar," *Progress In Electromagnetics Research*, Vol. 129, 287–313, 2012.

16. Liu, Q., "An accurate algorithm for nonuniform fast Fourier transforms (NUFFT's)," *IEEE Microwave and Guided Wave Letters*, Vol. 8, No. 1, 18–20, Jan. 1998.

17. Zhang, Y., W. Zhai, X. Zhang, X. Shi, X. Gu, and Y. Deng, "Ground moving train imaging by KU-band radar with two

receiving channels," *Progress In Electromagnetics Research*, Vol. 130, 493–512, 2012.

18. Park, S. H., J. I. Park, and K. T. Kim, "Motion compensation for squint mode spotlight SAR imaging using efficient 2D interpolation," *Progress In Electromagnetics Research*, Vol. 128, 503–518, 2012.

19. Li, Y., M. Xing, J. Su, Y. Quan, and Z. Bao, "A new algorithm of ISAR imaging for maneuvering targets with low SNR," *IEEE Trans. Aerosp. Electron. Syst.*, Vol. 49, No. 1, 543–557, Nov. 2013.

20. Park, S. H., J. H. Lee, and K. T. Kim, "Performance analysis of the scenario-based construction method for real target ISAR recognition," *Progress In Electromagnetics Research*, Vol. 128, 137–151, 2012.

21. Park, J. H. and N. H. Myung, "Enhanced and efficient ISAR imaging focusing using the discrete gabor representation in an oversampling scheme," *Progress In Electromagnetics Research*, Vol. 138, 227–244, 2013.

22. Golden, S. and B. Friedlander, "Estimation and statistical analysis of exponential polynomial signals," *IEEE Trans. Signal Process.*, Vol. 46, No. 11, 3127–3130, Nov. 1998.